Journal of Alloys and Compounds 509 (2011) 3274–3281

Contents lists available at ScienceDirect

Journal of Alloys and Compounds

journal homepage: www.elsevier.com/locate/jallcom

Thermodynamic description of the Mg–Nd–Zn ternary system

H.Y. Qi[a], G.X. Huang[a], H. Bo[a], G.L. Xu[a], L.B. Liu[a,b,c,*], Z.P. Jin[a,b,c]

[a] School of Material Science and Engineering, Central South University, Changsha, Hunan 410083, PR China
[b] Education Ministry Key Laboratory of Non-ferrous Materials Science and Engineering, Central South University, Changsha, Hunan 410083, PR China
[c] Center of Phase Diagram & Materials Design and Manufacture, Changsha, Hunan 410083, PR China

ARTICLE INFO

Article history:
Received 18 April 2010
Received in revised form 7 July 2010
Accepted 7 July 2010
Available online 15 July 2010

Keywords:
Mg–Nd–Zn system
CALPHAD method
Order–disorder transition

ABSTRACT

A thermodynamic description of the Mg–Nd–Zn system was developed by means of the CALPHAD (CALculation of PHAse Diagrams) method. The constituent binary systems Mg–Nd and Nd–Zn were re-optimized based on the experimental phase equilibria and thermodynamic properties available in the literature. Combining with the thermodynamic parameters of the Mg–Zn system cited from the reference, the Mg–Nd–Zn ternary system was evaluated. The Gibbs energies of the solution phases (liquid, BCC_A2, DHCP, HCP_A3 and HCP_Zn) were described by the subregular solution model with the Redlich–Kister polynomial function, and those of the stoichiometric compounds, Nd_2Zn_{17}, $NdZn_{11}$_H, $NdZn_{11}$_L, Nd_3Zn_{22}, $Nd_{13}Zn_{58}$, Nd_3Zn_{11}, $NdZn_3$, $NdZn_2$ and Mg_2Nd, were described by the sublattice model. The compounds Mg_3Nd and $Mg_{41}Nd_5$ in the Mg–Nd–Zn system were treated as the formulae $(Mg, Zn)_3(Mg, Nd)$ and $(Mg, Nd, Zn)_{41}(Mg, Nd)_5$. The order–disorder transition between BCC_B2 and BCC_A2 phases was treated using a two-sublattice model $(Mg, Nd, Zn)_{0.5}(Mg, Nd, Zn)_{0.5}$. Based on experimental data, four stable ternary compounds $\tau_1(Mg_7Nd_1Zn_{12})$, $\tau_2(Mg_7Nd_2Zn_{11})$, $\tau_3(Mg_6Nd_1Zn_3)$ and $\tau_4(Mg_6Nd_3Zn_{11})$ were taken into consideration in this system. A set of self-consistent thermodynamic parameters of the Mg–Nd–Zn system was obtained. Projection of the liquidus surface, selected vertical and isothermal sections were calculated using the proposed thermodynamic description. Comprehensive comparisons between the calculated and measured phase diagrams show that almost all the accurate experimental information is satisfactorily accounted for by the present thermodynamic description.

1. Introduction

With the increased worldwide emphasis on improved fuel efficiency, magnesium alloys are widely used in the automotive, communications and aerospace industries because of their advantageous properties such as low density, high specific strength, good castability, excellent machinability and good weldability [1–8]. However, compared with other metals such as aluminum or steel, the applications of magnesium alloys are limited owing to their restrained mechanical properties and creep resistance at elevated temperatures [1–4]. The addition of rare earth elements has been reported to be an effective method for improving creep resistance and mechanical properties of magnesium alloys at elevated temperatures [4–8]. Among the mischmetal (MM, including Ce, La, Nd, Pr, etc.), Nd has the greatest solubility in magnesium based solid solution [9]. The addition of Nd to Mg alloys results in a significantly increase on hardness and strength after suitable heat treatment due to the formation of plate-shaped GP zones and precipitates on prismatic planes of the Mg matrix [10]. The addition of Zn to a binary Mg–Nd alloy would further increase its peak-aged hardness. Wilson et al. [10] systematically investigated the effects of Zn additions on the precipitate microstructures, ageing behavior and mechanical properties of Mg–Nd alloy. Despite these interesting results, the mechanism why the rare earth elements can improve the performance of the magnesium alloys has not been clearly identified. Phase relations of the Mg–Nd–Zn system are particularly helpful for alloy design. The present work aims to develop a consistent thermodynamic description of the Mg–Nd–Zn system using the CALPHAD technique. In this work, the thermodynamic parameters for the Mg–Nd and Nd–Zn binary systems were re-optimized. Combining with the parameters of the Mg–Zn system cited from the reference [11], the Mg–Nd–Zn ternary system was optimized based on available experimental data.

2. Experimental data from the literature

2.1. Mg–Nd system

The Mg–Nd phase diagram was first constructed by Nayeb-Hashemi and Clark [12] according to early investigations [13–16]

* Corresponding author at: School of Material Science and Engineering, Central South University, Changsha, Hunan 410083, PR China. Tel.: +86 73188877732; fax: +86 73188876692.
E-mail address: pdc@mail.csu.edu.cn (L.B. Liu).

0925-8388/$ – see front matter © 2010 Elsevier B.V. All rights reserved.
doi:10.1016/j.jallcom.2010.07.056

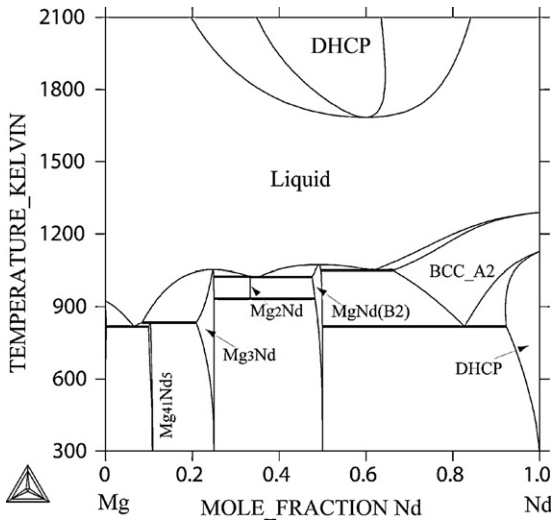

Fig. 1. Calculated Mg–Nd phase diagram using the thermodynamic description determined by Guo et al. [22,23].

and the assumed similarities with Mg–La, Mg–Ce and Mg–Pr systems. A systematic investigation of the Mg–Nd phase diagram was performed by Delfino et al. [17] using DTA, X-ray diffraction, metallography and microprobe analysis. Based on the experimental results of Delfino et al. [17], Okamoto [18] has redrawn the Mg–Nd phase diagram. Nayeb-Hashemi and Clark [12] have reported thermodynamic data of intermediate phases on the basis of vapor pressure measurements by Ogren et al. [19] and Pahlman and Smith [20].

Based upon the above-mentioned experimental data, the Mg–Nd system has been optimized by Gorsse et al. [21], Guo et al. [22,23] and Meng et al. [24]. Gorsse et al. [21] calculated the Mg–Nd system using substitutional solution model and associated model for the liquid phase. The optimized results showed that better agreement was obtained by using the associated model. However, the homogeneity range of intermetallic compounds and the order–disorder transformation between BCC_B2 and BCC_A2 phases were not considered. Later, Guo et al. [22,23] and Meng et al. [24] reassessed the Mg–Nd system. A calculation of the Mg–Nd system above 1685 K showed that the DHCP phase becomes stable as shown in Fig. 1 using the optimized parameters of Guo et al. [22,23]. The parameters of Meng et al. [24] have the same problem. In view of these facts, the Mg–Nd system was re-optimized using the Redlich–Kister polynomial to model the liquid phase. This was done to maintain the consistency with the other binaries Mg–Zn and Nd–Zn.

2.2. Nd–Zn system

On the basis of the experimental data [25], Qi et al. [26], Li et al. [27] and Liu et al. [28] have optimized the Nd–Zn system thermodynamically, however, the order–disorder transition between BCC_B2 and BCC_A2 phases was not considered in all these literatures. In the present work, the thermodynamic description of the Nd–Zn system was modified based on the thermodynamic parameters of Qi et al. [26].

2.3. Mg–Nd–Zn system

To facilitate reading, the symbols denoting the phases in the Mg–Nd–Zn system are listed in Table 1.

The phase relations of the Mg–Nd–Zn ternary system have been studied by Drits et al. [29,30] using metallography and thermal

Table 1
List of the symbols to denote the phases in the Mg–Nd–Zn system.

Symbol	Phase
L	Liquid
(Mg),(Nd),(Zn)	Solid solutions based on HCP_A3 Mg, DHCP Nd, HCP_Zn Zn, respectively
BCC_A2	Disordered bcc phase
BCC_B2	An ordered phase based on the bcc structure
$Mg_{51}Zn_{20}$	Binary $Mg_{51}Zn_{20}$ compound
MgZn	Binary MgZn compound
Mg_2Zn_3	Binary Mg_2Zn_3 compound
C14	Binary Mg_2Zn compound
Mg_2Zn_{11}	Binary Mg_2Zn_{11} compound
$NdZn_2$	Binary $NdZn_2$ compound
$NdZn_3$	Binary $NdZn_3$ compound
Nd_3Zn_{11}	Binary Nd_3Zn_{11} compound
$Nd_{13}Zn_{58}$	Binary $Nd_{13}Zn_{58}$ compound
Nd_3Zn_{22}	Binary Nd_3Zn_{22} compound
Nd_2Zn_{17}	Binary Nd_2Zn_{17} compound
$NdZn_{11}$_L	Binary $NdZn_{11}$_L compound
$NdZn_{11}$_H	Binary $NdZn_{11}$_H compound
Mg_2Nd	Binary Mg_2Nd compound
Mg_3Nd	Solid solution based on the Mg_3Nd phase
$Mg_{41}Nd_5$	Solid solution based on the $Mg_{41}Nd_5$ phase
$\tau_1(Mg_7Nd_1Zn_{12})$	Ternary compound
$\tau_2(Mg_7Nd_2Zn_{11})$	Ternary compound
$\tau_3(Mg_6Nd_1Zn_3)$	Ternary compound
$\tau_4(Mg_6Nd_3Zn_{11})$	Ternary compound

analysis. In Drits et al. [29], five vertical sections were studied, but only three of them, that at 10 wt.% Nd, at 20 wt.% Zn and from 80 wt.% Mg–20 wt.% Nd to 70 wt.% Mg–30 wt.% Zn were reported. Also a partial liquidus projection in the Mg-rich corner indicating four invariant reactions was given. Drits et al. [30] reported three isothermal sections at 473 K, 523 K and 573 K. Later, Drits et al. [31] reproduced the isothermal sections at 473 K and 573 K from Drits et al. [30] and gave the isothermal sections at 673 K and 773 K. Additionally, the compositions of the three ternary phases, previously discovered by Drits et al. [30], were identified by X-ray spectral analysis. Drits et al. [31] quoted the compositions of the three ternary phases as $Mg_1Nd_4Zn_5$, $Mg_6Nd_2Zn_7$ and $Mg_2Nd_2Zn_9$. A complete isothermal section at 573 K was established by Kinzhibalo et al. [32] based on XRD examination and they found four ternary phases, $Mg_7Nd_1Zn_{12}(\tau_1)$, $Mg_7Nd_2Zn_{11}(\tau_2)$, $Mg_6Nd_1Zn_3(\tau_3)$ and $Mg_6Nd_3Zn_{11}(\tau_4)$. The ternary compounds reported by these two groups [31] and [32] were totally different at nearly the same temperature. The isothermal sections given by Drits et al. [30,31] do not confirm the stated compositions of the ternary compounds as given by Drits et al. [31]. The compositions of the ternary phases determined by Drits et al. [31] were not used in the modeling. Recently, Huang et al. studied the phase equilibrium relationships in the Mg-rich corner at 573 K [33,34], 623 K [34] and 673 K [34,35]. The compositions and crystal structures of the phases in the Mg–Zn–Nd system were identified by scanning electron microscopy, electron probe microanalysis, X-ray diffraction and selected area electron diffraction of transmission electron microscopy. Two ternary compounds were identified by Huang et al. [33]. The composition range of one ternary phase is 58.3–63.9 at.% Mg, 28.2–33.6 at.% Zn and 7.9–8.3 at.% Nd. This is in agreement with that of τ_3 determined by Kinzhibalo et al. [32]. The composition range of the other phase is 25.9–30.3 at.% Mg, 44.6–48.5 at.% Zn and 25.1–25.6 at.% Nd. This is not a compound but a solid solution of Mg_3Nd containing the Zn element. The existence of τ_1 phase was also confirmed by Huang et al. [34]. The results obtained by Kinzhibalo et al. [32] and by Huang et al. [33–35] agree well with each other in terms of the homogeneity ranges of ternary phases and the phase equilibria. The isothermal

section at 573 K determined by Kinzhibalo et al. [32] was accepted in the present work. Additionally, the phases $NdZn_{11}$_L, Nd_3Zn_{22}, $Nd_{13}Zn_{58}$ and Nd_3Zn_{11} were added to the isothermal section. The $Mg_{51}Zn_{20}$ phase was excluded because it is not stable at 573 K.

Drits et al. [30] showed that there is a pseudo-binary eutectic reaction on the vertical section from the Mg solid solution to the τ_3 compound. It occurs at 798 K and the eutectic point is at 31 wt.% Nd, 10 wt.% Zn. This information is used in the optimization since it is generally believed that the measured eutectic temperature is more accurate than the measured liquidus. Due to the inconsistencies of composition ranges of ternary phases given by Drits et al. [31] and Kinzhibalo et al. [32], the vertical section from 80 wt.% Mg–20 wt.% Nd to 70 wt.% Mg–30 wt.% Zn should be corrected taking into account the isothermal sections. The invariant equilibria derived from the liquidus surface reported by Drits et al. [29] were utilized in the modeling.

3. Thermodynamic models

For a pure element with a certain structure Φ, its Gibbs energy function is described by the following equation:

$$^0G_i^{\Phi}(T) = a + bT + cT\ \ln T + dT^2 + eT^3 + fT^{-1} + gT^7 + hT^{-9} \quad (1)$$

where the parameters a through h are assigned from the SGTE Database [36].

The Gibbs energy of the element i (i = Mg, Nd, Zn), $^0G_i^{\Phi}(T)$, in a standard element reference (SER) state, is denoted by $GHSER_i$,

$$GHSER_i = {}^0G_i^{\Phi}(T) - H_i^{SER}(298.15\ K) \quad (2)$$

where $H_i^{SER}(298.15\,K)$ is the molar enthalpy of the element i at 298.15 K in its reference state, i.e. HCP_A3 for Mg, DHCP for Nd and HCP_Zn for Zn.

There are solution phases, stoichiometric intermetallic compounds and intermetallic compounds with noticeable solubility ranges in this alloy system. In the following part, the analytical expressions for all the phases are briefly presented.

3.1. Solution phases

The Gibbs energies for liquid, BCC_A2, HCP_A3, HCP_Zn and DHCP solution phases are described by the substitutional solution model as follows,

$$G^{\Phi} = \sum x_i^0 G_i^{\Phi} + RT\sum x_i \ln(x_i) + {}^EG_m^{\Phi} \quad (3)$$

where $^0G_i^{\Phi}$ is the molar Gibbs energy of the element i (i = Mg, Nd, Zn) with the structure Φ, R is the gas constant, T is the temperature expressed in K, x_i is the mole fractions of component i, and $^EG_m^{\Phi}$ is the excess Gibbs energy formulated with the Redlich–Kister polynomial [37] as

$$\begin{aligned} {}^EG_m^{\Phi} = {} & x_{Mg}x_{Nd}\sum_i {}^iL_{Mg,Nd}^{\Phi}(x_{Mg}-x_{Nd})^i + x_{Mg}x_{Zn}\sum_i {}^iL_{Mg,Zn}^{\Phi}(x_{Mg}-x_{Zn})^i \\ & + x_{Nd}x_{Zn}\sum_i {}^iL_{Nd,Zn}^{\Phi}(x_{Nd}-x_{Zn})^i + x_{Mg}x_{Nd}x_{Zn}\,{}^iL_{Mg,Nd,Zn}^{\Phi} \end{aligned} \quad (4)$$

where $^iL_{Mg,Nd}^{\Phi}$, $^iL_{Mg,Zn}^{\Phi}$ and $^iL_{Nd,Zn}^{\Phi}$ are the interaction parameters between elements Mg and Nd, Mg and Zn, and Nd and Zn, respectively; $^iL_{Mg,Nd,Zn}^{\Phi}$ is the ternary interaction parameter; $^iL_{Mg,Nd}^{\Phi}$, $^iL_{Nd,Zn}^{\Phi}$ and $^iL_{Mg,Nd,Zn}^{\Phi}$ are to be evaluated in the present work. The general form of the interaction parameters is:

$$L^{\Phi} = a + bT + cT\ \ln T + dT^2 + eT^3 + fT^{-1} \quad (5)$$

In most cases, only the first one or two terms are used according to the temperature dependence of the experimental data.

3.2. Intermetallic compounds

In the binary systems, $Mg_{41}Nd_5$ and Mg_3Nd are described with the sublattice models (**Mg**, Nd)$_{41}$(Mg, **Nd**)$_5$ and **Mg**$_3$(Mg, **Nd**)$_1$, respectively, where boldface **Mg** and **Nd** represent the major species in the sublattices. Because of the remarkable solubilities of Zn in $Mg_{41}Nd_5$ and Mg_3Nd, the sublattice models (Mg, Nd, Zn)$_{41}$(Mg, Nd)$_5$ and (Mg, Zn)$_3$(Mg, Nd)$_1$ are employed. A detailed review of the sublattice model can be found in [38]. As an example, for a two sublattice phase Φ, $(A_{y'_A}B_{y'_B})_p(A_{y''_A}B_{y''_B})_q$ with the subscripts p and q referring to total number of sites on each sublattice,

$$G_{\Phi}^{ref} = y'_Ay''_AG^0_{A:A} + y'_Ay''_BG^0_{A:B} + y'_By''_AG^0_{B:A} + y'_By''_BG^0_{B:B} \quad (6)$$

where $G^0_{A:B}$ refers to the Gibbs energy of a hypothetical compound A_pB_q and $y'_Ay''_B$ the corresponding product of the site fractions. Other terms in Eq. (6) can be interpreted in a similar way.

The Gibbs energy of the sublattice model for a phase Φ is expressed as:

$$G^{\Phi} = G_{\Phi}^{ref} + G_{\Phi}^{id} + G_{\Phi}^{E} \quad (7)$$

The ideal mixing term G_{Φ}^{id} is,

$$G_{\Phi}^{id} = RT[p(y'_A\ \ln y'_A + y'_B\ln y'_B) + q(y''_A\ln y''_A + y''_B\ln y''_B)] \quad (8)$$

The excess Gibbs energy is,

$$\begin{aligned} G_{\Phi}^{E} = {} & y'_Ay'_B[y''_AL_{A,B:A} + y''_BL_{A,B:B}] + y''_Ay''_B[y'_AL_{A:A,B} + y'_{B:A,B}] \\ & + y'_Ay'_By''_Ay''_BL_{A,B:A,B} \end{aligned} \quad (9)$$

with the interaction parameter e.g. $L_{A,B:A}$ and $L_{B:A,B}$ denoting mixing on only one of the sites.

3.3. Ordered BCC_B2 phase

In order to represent the Gibbs energies of both the disordered BCC_A2 phase, described by a model (Mg, Nd, Zn), and the ordered BCC_B2 phase using a single function, the BCC_B2 phase is modeled as (Mg, Nd, Zn)$_{0.5}$(Mg, Nd, Zn)$_{0.5}$. Ansara et al. [39] have derived an equation which allows the thermodynamic properties of the disordered phase to be evaluated independently. This is done by dividing the Gibbs energy into three terms:

$$\begin{aligned} G_m^{BCC\_A2,B2} = {} & G_m^{BCC\_A2}(x_{Mg}, x_{Nd}, x_{Zn}) \\ & + G_m^{B2}(y'_{Mg}, y'_{Nd}, y'_{Zn}, y''_{Mg}, y''_{Nd}, y''_{Zn}) - G_m^{B2}(x_{Mg}, x_{Nd}, x_{Zn}) \end{aligned} \quad (10)$$

where y'_{Mg}, y'_{Nd}, and y'_{Zn} are the site fractions of Mg, Nd and Zn in the first sublattice, and y''_{Mg}, y''_{Nd} and y''_{Zn} are those in the second one. $G_m^{BCC\_A2}(x_{Mg}, x_{Nd}, x_{Zn})$ is the Gibbs energy of the disordered BCC_A2 phase. The second term, $G_m^{B2}(y'_{Mg}, y'_{Nd}, y'_{Zn}, y''_{Mg}, y''_{Nd}, y''_{Zn})$, is described by the sublattice model and implicitly contains a contribution from the disordered state. The last term, $G_m^{B2}(x_{Mg}, x_{Nd}, x_{Zn})$, represents that contribution from the disordered state to the ordered one. When the site fractions are equal, i.e. $y'_{Mg} = y''_{Mg}$, $y'_{Nd} = y''_{Nd}$ and $y'_{Zn} = y''_{Zn}$, the last two terms cancel each other. In this case, Eq. (10) corresponds to the disordered state.

3.4. Stoichiometric phases

Because of the negligible solid solubilities for the third element, $NdZn_2$, $NdZn_3$, Nd_3Zn_{11}, $Nd_{13}Zn_{58}$, Nd_3Zn_{22}, Nd_2Zn_{17}, $NdZn_{11}$_H, $NdZn_{11}$_L and Mg_2Nd are treated as stoichiometric phases. Four ternary compounds, τ_1-$Mg_7Nd_1Zn_{12}$, τ_2-$Mg_7Nd_2Zn_{11}$, τ_3-$Mg_6Nd_1Zn_3$, and τ_4-$Mg_6Nd_3Zn_{11}$, were modeled as stoichiometric

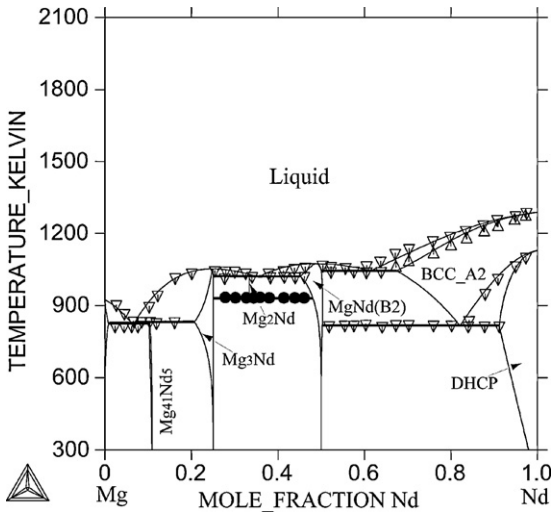

Fig. 2. Calculated Mg–Nd phase diagram using the present thermodynamic description compared with the experimental data [17]. (●) Thermal effects observed on heating and cooling; (▽) thermal effects observed on cooling; (△) thermal effects observed on heating.

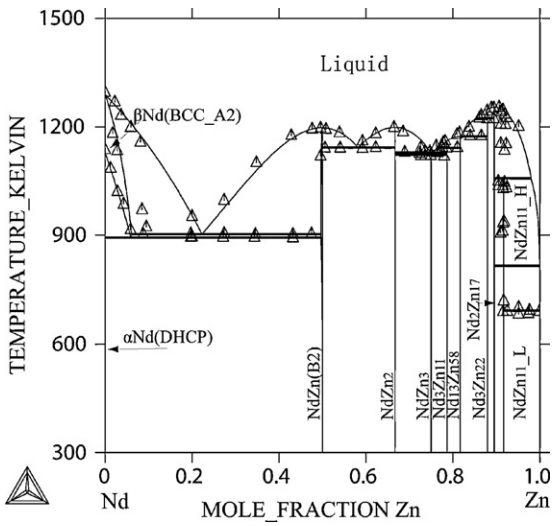

Fig. 4. Calculated Nd–Zn phase diagram using the present thermodynamic description compared with the experimental data [25].

phases ($Mg_xNd_yZn_z$), and their Gibbs energy expressions are written as:

$$G_{Mg_xNd_yZn_z} = xG_{Mg}^{HCP\_A3} + yG_{Nd}^{DHCP} + zG_{Zn}^{HCP\_ZN} + C + DT \quad (11)$$

where C and D are the parameters to be optimized.

4. Results and discussion

On the basis of lattice stabilities taken from the PURE database [36], the optimization of the Mg–Nd and Nd–Zn system is carried out using the PARROT module in the Thermo-Calc software package developed by Sundman et al. [38]. The phase diagram and thermochemical literature data have been used as input to the program for the optimization.

The calculated Mg–Nd phase diagram using the thermodynamic parameters from Guo et al. [22,23] is shown in Fig. 1. The DHCP phase is stable at higher temperatures. The Mg–Nd binary system was re-optimized in this work. The calculated Mg–Nd phase diagram compared with the experimental data [17] is shown in Fig. 2.

All the invariant reactions in the Mg–Nd system compared with that reported by the literature [17] are listed in Table 2. The calculated liquidus and invariant reactions are in good agreement with the experimental data [17]. The comparison of Gibbs energies of formation at 773 K between the calculated results and experimental data [20] is shown in Fig. 3. The calculated Gibbs energies of formation of all the compounds are consistent with experimental values except for $Mg_{41}Nd_5$. The formation of $Mg_{41}Nd_5$ peritectically may result in the presence of a small amount of nonequilibrium phase in the prepared alloys. The discrepancy is accepted in order to fit the phase diagram data for the $Mg_{41}Nd_5$ phase better.

The calculated Nd–Zn phase diagram compared with the experimental data [25] is presented in Fig. 4. Compared with the result of the previous work [26], the order–disorder transition between BCC_B2 and BCC_A2 was included. All the invariant reactions in the Nd–Zn system are listed in Table 3. The differences between the calculated and experimentally determined temperatures for the invariant reactions are within the error limit.

Combining the optimized results of Mg–Nd and Nd–Zn binary systems in this work with that of the Mg–Zn system cited from the reference, the Mg–Nd–Zn ternary system was optimized based

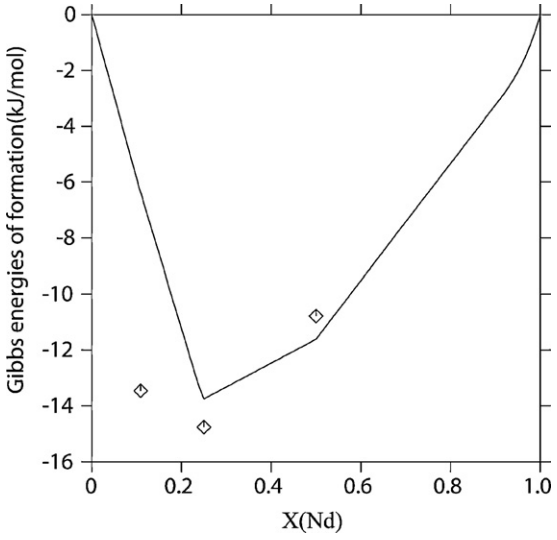

Fig. 3. Calculated Gibbs energies of formation at 773 K in Mg–Nd system compared with experimental data [20] (Ref. state: Mg, HCP_A3; Nd, DHCP).

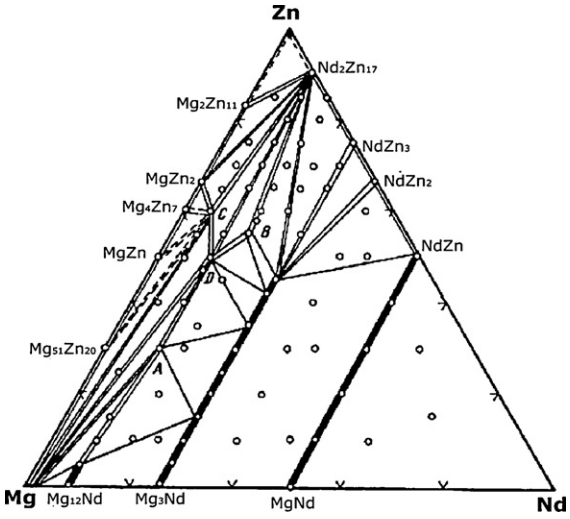

Fig. 5. The experimental isothermal section of Mg–Nd–Zn system at 573 K by Kinzhibalo et al. [32].

Table 2
Invariant reactions in the Mg–Nd system.

Reaction	T(K)		Phases	Comp. (at.% Nd)	
	Exp [17]	Cal		Exp [17]	Cal
L → MgNd(B2) + BCC_A2	1048	1045	Liquid	57.5	61.5
			B2	–	50.0
			BCC_A2	66.0	67.4
L + Mg_3Nd → Mg_2Nd	>1023	1023	Liquid	–	34.7
			Mg_3Nd	–	25.0
			Mg_2Nd	–	33.3
L → Mg_2Nd + MgNd(B2)	1023	1022	Liquid	35.5	35.8
			Mg_2Nd	–	33.3
			B2	–	45.1
Mg_2Nd → Mg_3Nd + MgNd(B2)	933	930	Mg_3Nd	–	25.0
			Mg_2Nd	–	33.3
			B2	–	48.1
L + Mg_3Nd → $Mg_{41}Nd_5$	833	832	Liquid	8.5	7.0
			Mg_3Nd	–	20.6
			$Mg_{41}Nd_5$	–	10.3
L → $Mg_{41}Nd_5$ + HCP_A3	818	826	Liquid	7.5	6.2
			$Mg_{41}Nd_5$	–	10.2
			HCP_A3	0.1	0.8
BCC_A2 → MgNd(B2) + DHCP	818	816	BCC_A2	83.0	82.1
			B2	–	50.3
			DHCP	92.0	91.1

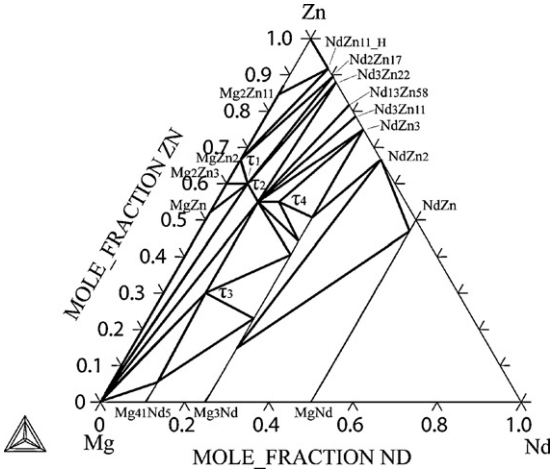

Fig. 6. Calculated isothermal section of the Mg–Nd–Zn system at 573 K.

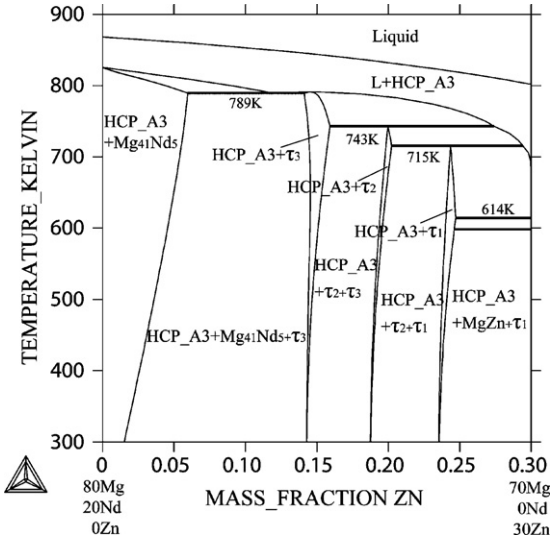

Fig. 7. Calculated vertical section from 80 wt.% Mg–20 wt.% Nd to 70 wt.% Mg–30 wt.% Zn.

Table 3
Invariant reactions in the Nd–Zn system.

Reaction	T(K)		Composition, x^L_{Zn} (at.%)	
	Exp [25]	Cal	Exp [25]	Cal
L + Nd_2Zn_{17} → Nd_3Zn_{22}	1223	1225	–	85.3
L → $Nd_{13}Zn_{58}$ + Nd_3Zn_{22}	1175	1174	–	81.8
L → NdZn(B2) + $NdZn_2$	1141	1142	57.5	58.2
L + $Nd_{13}Zn_{58}$ → Nd_3Zn_{11}	1143	1141	–	76.9
L → $NdZn_2$ + Nd_3Zn_{11}	1127	1128	73.7	74.8
$NdZn_2$ + Nd_3Zn_{11} → $NdZn_3$	1122	1122	–	–
L + Nd_2Zn_{17} → $NdZn_{11}$_H	1053	1057	–	98.0
L → NdZn(B2) + BCC_A2	903	902	23.0	22.3
BCC_A2 → NdZn(B2) + DHCP	895	893	–	–
L + $NdZn_{11}$_L → HCP_Zn	693	693	≈1	99.9

Table 4
Thermodynamic parameters in the Mg–Nd–Zn system.

Phase	Thermodynamic parameters	Ref.
Liquid model: $(Mg, Nd, Zn)_1$	${}^0L^{Liq}_{Mg,Nd} = -34308.7 + 10.9T$	This work
	${}^1L^{Liq}_{Mg,Nd} = -14565.6$	This work
	${}^2L^{Liq}_{Mg,Nd} = -16479.0$	This work
	${}^0L^{Liq}_{Mg,Zn} = -77729.24 + 680.52266T - 95T\ \ln(T) + 0.04T^2$	[11]
	${}^1L^{Liq}_{Mg,Zn} = 3674.72 + 0.57139T$	[11]
	${}^2L^{Liq}_{Mg,Zn} = -1588.15$	[11]
	${}^0L^{Liq}_{Nd,Zn} = -101981.93 + 20.0T$	This work
	${}^1L^{Liq}_{Nd,Zn} = +76182.7 - 29.9T$	This work
	${}^2L^{Liq}_{Nd,Zn} = -31990 + 18.0T$	This work
BCC_A2 (disordered part of Bcc_B2): $(Mg, Nd, Zn)_1(Va)_3$	${}^0L^{BCC\_A2}_{Mg,Nd} = -24721.4 + 1.5T$	This work
	${}^1L^{BCC\_A2}_{Mg,Nd} = -25696.4 + 8.3T$	This work
	${}^2L^{BCC\_A2}_{Mg,Nd} = -16898.5$	This work
	${}^0L^{BCC\_A2}_{Nd,Zn} = -46975.5 + 3.2T$	This work
	${}^0L^{BCC\_A2}_{Mg,Nd,Zn} = -15000$	This work
BCC_B2 $(Mg, Nd, Zn)_{0.5}(Mg, Nd, Zn)_{0.5}$	${}^0L^{BCC\_B2}_{Mg:Nd} = {}^0L^{BCC\_B2}_{Nd:Mg} = -26755 + 2.9T$	This work
	${}^0L^{BCC\_B2}_{Mg,Nd:Nd} = {}^0L^{BCC\_B2}_{Nd:Mg,Nd} = -21500$	This work
	${}^1L^{BCC\_B2}_{Mg,Nd:Nd} = {}^1L^{BCC\_B2}_{Nd:Mg,Nd} = +12000$	This work
	${}^0L^{BCC\_B2}_{Nd:Zn} = {}^0L^{BCC\_B2}_{Zn:Nd} = -39405.4 + 7.8T87$	This work
	${}^0L^{BCC\_B2}_{Nd,Zn:Nd} = {}^0L^{BCC\_B2}_{Nd:Nd,Zn} = +12000$	This work
	${}^1L^{BCC\_B2}_{Nd,Zn:Nd} = {}^1L^{BCC\_B2}_{Nd:Nd,Zn} = -6000$	This work
DHCP model: $(Mg, Nd, Zn)_1$	${}^0G^{DHCP}_{Mg} = 303.4 + GHSERMG$	[22]
	${}^0L^{DHCP}_{Mg,Nd} = +22713.0 - 5.6T$	This work
	${}^1L^{DHCP}_{Mg,Nd} = +38913.4$	This work
HCP_A3 model: $(Mg, Nd, Zn)_1(Va)_{0.5}$	${}^0G^{HCP\_A3}_{Nd} = 303.4 + GHSERND$	[22]
	${}^0G^{HCP\_A3}_{Zn} = GHSERZN$	[36]
	${}^0L^{HCP\_A3}_{Mg,Nd} = -18000$	This work
	${}^1L^{HCP\_A3}_{Mg,Nd} = -7000$	This work
	${}^0L^{HCP\_A3}_{Mg,Zn} = -3056.82 + 5.63801T$	[11]
	${}^1L^{HCP\_A3}_{Mg,Zn} = -3127.26 + 5.65563T$	[11]
HCP_ZN model: $(Mg, Nd, Zn)_1(Va)_{0.5}$	${}^0G^{HCP\_ZN}_{Zn} = GHSERZNR$	[36]
	${}^0L^{HCP\_Zn}_{Mg,Zn} = -3056.82 + 5.63801T$	[11]
	${}^1L^{HCP\_Zn}_{Mg,Zn} = -3127.26 + 5.65563T$	[11]
$Mg_{51}Zn_{20}$ model: $(Mg)_{51}(Zn)_{20}$	$G^{Mg_{51}Zn_{20}}_{Mg:Zn} = -335741.54 + 35.5T + 51GHSERMG + 20GHSERZNR$	[11]
MgZn model: $(Mg)_{12}(Zn)_{13}$	$G^{MgZn}_{Mg:Zn} = -236980.84 + 59.24524T + 12GHSERMG + 13GHSERZNR$	[11]
Mg_2Zn_3 model: $(Mg)_2(Zn)_3$	$G^{Mg_2Zn_3}_{Mg:Zn} = -54406.2 + 13.60156T + 2GHSERMG + 3GHSERZNR$	[11]
Laves_C14 model: $(Mg,Zn)_2(Mg,Zn)_1$	$G^{C14}_{Mg:Mg} = 15000 + 3GHSERMG$	[11]
	$G^{C14}_{Zn:Zn} = 15000 + 3GHSERZNR$	[11]
	$G^{C14}_{Zn:Mg} = -35355.45 + 8.83886 + 2GHSERZNR + GHSERMG$	[11]
	$G^{C14}_{Mg:Zn} = +65355.45 - 8.83886 + GHSERZNR + 2GHSERMG$	[11]
	$G^{C14}_{Mg,Zn:Mg} = G^{C14}_{Mg,Zn:Zn} = 35000$	[11]
	$G^{C14}_{Mg:Mg,Zn} = G^{C14}_{Zn:Mg,Zn} = 8000$	[11]
Mg_2Zn_{11} model: $(Mg)_2(Zn)_{11}$	$G^{Mg_2Zn_{11}}_{Mg:Zn} = -73818.32 + 18.45457T + 2GHSERMG + 11GHSERZNR$	[11]
$NdZn_2$ model: $(Nd)_{0.333}(Zn)_{0.667}$	$G^{NdZn_2}_{Nd:Zn} = -39154.2 + 7.2T + 0.333GHSERND + 0.667GHSERZNR$	This work
$NdZn_3$ model: $(Nd)_{0.25}(Zn)_{0.75}$	$G^{NdZn_3}_{Nd:Zn} = -37764.8 + 8.7T + 0.25GHSERND + 0.75GHSERZNR$	This work
Nd_3Zn_{11} model: $(Nd)_{0.214}(Zn)_{0.786}$	$G^{Nd_3Zn_{11}}_{Nd:Zn} = -34736.0 + 7.2T + 0.214GHSERND + 0.786GHSERZNR$	This work
$Nd_{13}Zn_{58}$ model: $(Nd)_{0.183}(Zn)_{0.817}$	$G^{Nd_{13}Zn_{58}}_{Nd:Zn} = -32198.0 + 6.1T + 0.183GHSERND + 0.817GHSERZNR$	This work
Nd_3Zn_{22} model: $(Nd)_{0.12}(Zn)_{0.88}$	$G^{Nd_3Zn_{22}}_{Nd:Zn} = -27399.9 + 5.3T + 0.12GHSERND + 0.88GHSERZNR$	This work
Nd_2Zn_{17} model: $(Nd)_{0.105}(Zn)_{0.895}$	$G^{Nd_2Zn_{17}}_{Nd:Zn} = -26208.7 + 5.3T + 0.105GHSERND + 0.895GHSERZNR$	This work
$NdZn_{11}$_L model: $(Nd)_{0.083}(Zn)_{0.917}$	$G^{NdZn_{11}\_L}_{Nd:Zn} = -22770.4 + 5.2T + 0.083GHSERND + 0.917GHSERZNR$	This work
$NdZn_{11}$_H model: $(Nd)_{0.083}(Zn)_{0.917}$	$G^{NdZn_{11}\_H}_{Nd:Zn} = -22694.6 + 5.2T + 0.083GHSERND + 0.917GHSERZNR$	This work
Mg_2Nd model: $(Mg)_2(Nd)_1$	$G^{Mg_2Nd}_{Mg:Nd} = -45530 + 9.0T + GHSERND + 2GHSERMG$	This work
Mg_3Nd model: $(Mg, Zn)_3(Mg, Nd)_1$	$G^{Mg_3Nd}_{Mg:Mg} = +12400 - 8.4T + 4GHSERMG$	This work
	$G^{Mg_3Nd}_{Mg:Nd} = -75831.5 + 26.9T + GHSERND + 3GHSERMG$	This work
	$G^{Mg_3Nd}_{Mg:Mg,Nd} = +7999.8$	This work
	$G^{Mg_3Nd}_{Zn:Nd} = -145000 + 34T + GHSERND + 3GHSERZNR$	This work
$Mg_{41}Nd_5$ model: $(Mg, Nd, Zn)_{41}(Mg, Nd)_5$	$G^{Mg_{41}Nd_5}_{Mg:Mg} = +138000 + 46GHSERMG$	This work

Table 4 (*Continued* **).**

Phase	Thermodynamic parameters	Ref.
	$G^{Mg_{41}Nd_5}_{Nd:Nd} = +138000 + 46GHSERND$	This work
	$G^{Mg_{41}Nd_5}_{Nd:Mg} = +459385.6 - 217.3T + 5GHSERMG + 41GHSERND$	This work
	$G^{Mg_{41}Nd_5}_{Mg:Nd} = -459385.6 + 217.3T + 41GHSERMG + 5GHSERND$	This work
	$G^{Mg_{41}Nd_5}_{Zn:Nd} = -1000000 + 240T + 41GHSERZNR + 5GHSERND$	This work
	${}^0G^{Mg_{41}Nd_5}_{Mg,Nd:Mg} = {}^0G^{Mg_{41}Nd_5}_{Mg,Nd:Nd} = -51679.8 + 10.2T$	This work
	${}^0G^{Mg_{41}Nd_5}_{Mg:Mg,Nd} = {}^0G^{Mg_{41}Nd_5}_{Nd:Mg,Nd} = -56137.8 + 3.7T$	This work
τ_1 model: $(Mg)_{0.35}$ $(Nd)_{0.05}$ $(Zn)_{0.60}$	$G^{\tau_1}_{Nd:Mg:Zn} = -16300 + 0.35GHSERMG + 0.05GHSERND + 0.60GHSERZNR$	This work
τ_2 model: $(Mg)_{0.35}$ $(Nd)_{0.1}$ $(Zn)_{0.55}$	$G^{\tau_2}_{Nd:Mg:Zn} = -19940 + 0.35GHSERMG + 0.1GHSERND + 0.55GHSERZNR$	This work
τ_3 model: $(Mg)_{0.6}$ $(Nd)_{0.1}$ $(Zn)_{0.3}$	$G^{\tau_3}_{Nd:Mg:Zn} = -14700 + 0.6GHSERMG + 0.1GHSERND + 0.3GHSERZNR$	This work
τ_4 model: $(Mg)_{0.3}$ $(Nd)_{0.15}$ $(Zn)_{0.55}$	$G^{\tau_4}_{Nd:Mg:Zn} = -23050 + 0.3GHSERMG + 0.15GHSERND + 0.55GHSERZNR$	This work

on available experimental data. Thermodynamic parameters for all the phases in the Mg–Nd–Zn ternary system are summarized in Table 4 . Table 5 lists all the invariant reactions in this ternary system. The experimental isothermal section of the Mg–Nd–Zn system at 573 K reported by Kinzhibalo et al. [32] is shown in Fig. 5. The calculated isothermal section at 573 K is presented in Fig. 6. The phases, $NdZn_{11}$_L, Nd_3Zn_{22}, $Nd_{13}Zn_{58}$ and Nd_3Zn_{11}, are included in the calculated isothermal section. The binary phases, MgNd and NdZn, form a complete solution phase BCC_B2. In order to fit the

Table 5
Calculated invariant points in the Mg–Nd–Zn ternary system compared with experimental data [29].

Type	Reaction	Temperature (K)	
		Calculated	Experimental
Saddle points			
Max_1	$L \rightarrow NdZn_2 + Mg_3Nd$	1088	
Max_2	$L \rightarrow Mg_3Nd + B2$	1082	
Max_3	$L \rightarrow Mg_3Nd + \tau_4$	1067	
Max_4	$L \rightarrow \tau_2 + \tau_4$	1060	
Max_5	$L \rightarrow \tau_4 + Nd_3Zn_{11}$	1056	
Max_6	$L \rightarrow \tau_4 + Nd_{13}Zn_{58}$	1055	
Max_7	$L \rightarrow \tau_4 + NdZn_3$	1054	
Max_8	$L \rightarrow \tau_1 + \tau_2$	1028	
Max_9	$L \rightarrow \tau_1 + Nd_2Zn_{17}$	1027	
Max_{10}	$L \rightarrow HCP\_A3 + \tau_3$	791	798 [29]
Ternary quasi-peritectic			
U_1	$L + Mg_3Nd \rightarrow NdZn_2 + \tau_4$	1062	
U_2	$L + \tau_4 \rightarrow \tau_2 + Nd_{13}Zn_{58}$	1041	
U_3	$L + Nd_{13}Zn_{58} \rightarrow \tau_2 + Nd_3Zn_{22}$	1036	
U_4	$L + Nd_2Zn_{17} \rightarrow \tau_1 + Nd_3Zn_{22}$	1027	
U_5	$L + \tau_4 \rightarrow \tau_3 + \tau_2$	882	
U_6	$L + \tau_1 \rightarrow C14 + Nd_2Zn_{17}$	863	
U_7	$L + Nd_2Zn_{17} \rightarrow C14 + NdZn_{11}\_H$	844	
U_8	$L + Mg_3Nd \rightarrow \tau_3 + Mg_{41}Nd_5$	804	
U_9	$L + \tau_3 \rightarrow \tau_2 + HCP\_A3$	743	746 [29]
U_{10}	$L + \tau_2 \rightarrow \tau_1 + HCP\_A3$	715	713 [29]
U_{11}	$L + NdZn_{11}\_L \rightarrow Mg_2Zn_{11} + HCP\_Zn$	640	
U_{12}	$L + \tau_1 \rightarrow Mg_7Zn_3 + MgZn$	614	
Ternary peritectic			
P_1	$L + Nd_3Zn_{11} + NdZn_2 \rightarrow NdZn_3$	1122	
P_2	$L + Mg_3Nd + \tau_4 \rightarrow \tau_3$	895	
P_3	$L + C14 + NdZn_{11}\_H \rightarrow NdZn_{11}\_L$	815	
P_4	$L + \tau_1 + C14 \rightarrow Mg_2Zn_3$	689	
P_5	$L + C14 + NdZn_{11}\_L \rightarrow Mg_2Zn_{11}$	654	
P_6	$L + Mg_2Zn_3 + \tau_1 \rightarrow MgZn$	620	
P_7	$L + \tau_1 + HCP\_A3 \rightarrow Mg_7Zn_3$	614	
Ternary eutectic			
E_1	$L \rightarrow B2 + Mg_3Nd + NdZn_2$	1060	
E_2	$L \rightarrow Nd_{13}Zn_{58} + Nd_3Zn_{11} + \tau_4$	1055	
E_3	$L \rightarrow Nd_3Zn_{11} + \tau_4 + NdZn_3$	1054	
E_4	$L \rightarrow NdZn_3 + NdZn_2 + \tau_4$	1053	
E_5	$L \rightarrow \tau_1 + Nd_3Zn_{22} + \tau_2$	1025	
E_6	$L \rightarrow B2 + Mg_3Nd + Mg_2Nd$	1020	
E_7	$L \rightarrow \tau_3 + Mg_{41}Nd_5 + HCP\_A3$	789.37	793 [29]

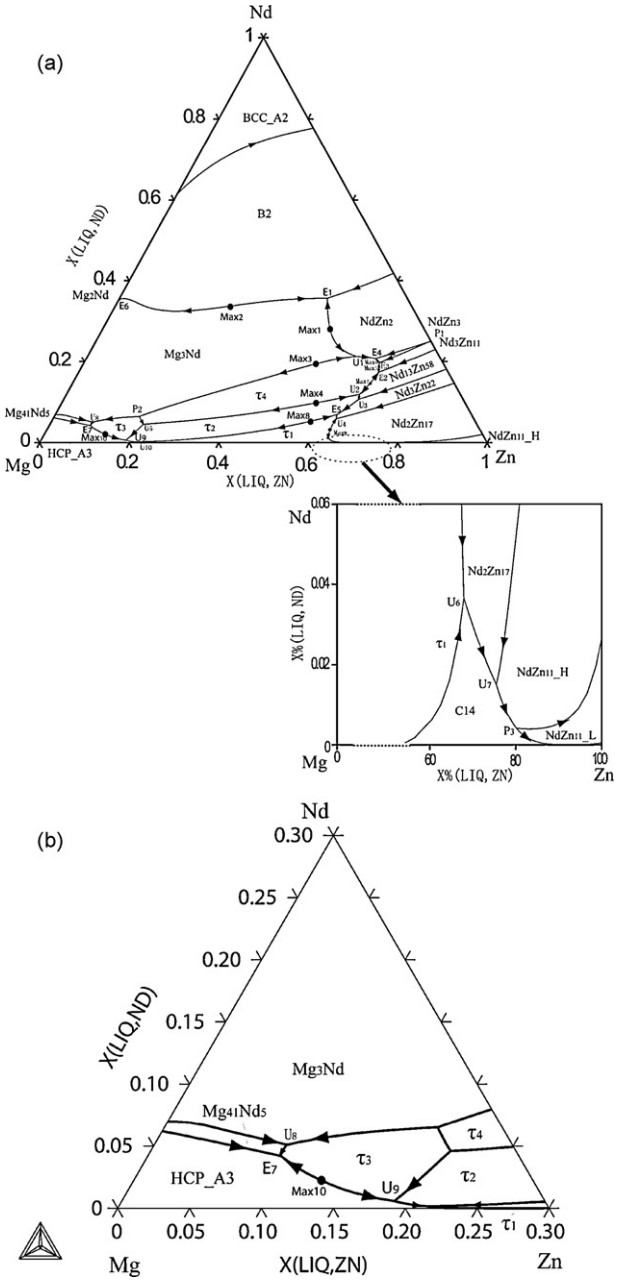

Fig. 8. Calculated liquidus projection of Mg–Nd–Zn system using the present thermodynamic description (a) full view (b) in the Mg-rich corner.

remarkable solubility of Zn in $Mg_{41}Nd_5$ and Mg_3Nd, the sublattice models $(Mg, Nd, Zn)_{41}(Mg, Nd)_5$ and $(Mg, Zn)_3(Mg, Nd)_1$ are employed in this work. Comparing with Fig. 5, the phase relations and phase boundaries of the calculated isothermal section agree well with the literature [32]. Fig. 7 shows the calculated vertical section of the Mg–Nd–Zn system from 80 wt.% Mg–20 wt.% Nd to 70 wt.% Mg–30 wt.% Zn. A shift of the phase boundaries occurs comparing to the experimental data [29]. The discrepancy between the calculated and experimental data was mainly caused by the inconsistency between the composition of the ternary compounds determined by Drits et al. [31] and Kinzhibalo et al. [32]. However, the calculated temperatures of the invariant reactions agree well with the experimental results determined by Drits et al. [29]. Fig. 8a and b are the calculated projection of the liquidus surface of the Mg–Nd–Zn system using the present thermodynamic description. The calculated temperatures of invariant reactions in the Mg-rich corner agree well with the experimental data [29] presented in Table 5.

The Mg–Nd–Zn ternary system should be further investigated experimentally.

5. Summary

The Mg–Nd and Nd–Zn systems have been re-optimized in this work. A reasonable thermodynamic description of the Mg–Nd–Zn system has been established based on the experimental information available in the literature. A set of self-consistent parameters capable of describing all phases in this ternary system has been obtained. The calculated liquidus projection and certain vertical and isothermal sections show good agreement with the reported experimental data.

Acknowledgements

This work was financially supported by the National Science Foundation of China (Grant No. 50731002), Center of Phase Diagram & Materials Design and Manufacture Foundation (Grant No. 1773-206001146), and Excellent PhD Thesis Support Foundation of Central South University (Grant No. 2008yb013).

References

[1] B.L. Mordike, T. Ebert, Mater. Sci. Eng. A 302 (2001) 37–45.
[2] L.L. Roklin, T.V. Dobatkina, N.I. Nikitina, Mater. Sci. Forum 419 (2003) 291–296.
[3] C. Antion, P. Donnadieu, C. Tassin, A. Pisch, Philos. Mag. 186 (2006) 2797–2810.
[4] X. Gao, J.F. Nie, Scr. Mater. 58 (2008) 619–622.
[5] P.H. Fu, L.M. Peng, H.Y. Jiang, L. Ma, C.Q. Zhai, Mater. Sci. Eng. A 496 (2008) 177–188.
[6] M. Eddahbi, P. Pérez, M.A. Monge, G. Garcés, R. Pareja, P. Adeva, J. Alloys Compd. 473 (2009) 79–86.
[7] G. Sha, J.H. Li, W. Xu, K. Xia, W.Q. Jie, S.P. Ringer, Mater. Sci. Eng. A 527 (2010) 5092–5099.
[8] N. Stanford, Mater. Sci. Eng. A 527 (2010) 2669–2677.
[9] L.L. Roklin, Magnesium Alloys Containing Rare Earth Metals, Taylor and Francis, London, 2003.
[10] R. Wilson, C.J. Bettles, B.C. Muddle, J.F. Nie, Mater. Sci. Forum 419–422 (2003) 267–272.
[11] P. Liang, T. Tarfa, J.A. Robinson, S. Wagner, P. Ochin, M.G. Harmelin, H.J. Seifert, H.L. Lukas, F. Aldinger, Thermochim. Acta 314 (1998) 87–110.
[12] A.A. Nayeb-Hashemi, J.B. Clark, Phase Diagrams of Binary Magnesium Alloys, ASM International, Metals Park, Ohio, 1998.
[13] R.R. Joseph, K.A. Gschneidner Jr., Trans. AIME 223 (1965) 2063–2069.
[14] R.R. Park, L.L. Wyman, WACD Tech. Rep. 33 (1957) 57–504.
[15] L.L. Rokhlin, Russ. Met. Fuels 2 (1962) 98–100.
[16] M.E. Drits, E.M. Padezhnova, N.V. Miklina, Russ. Metall. 1 (1971) 143–146.
[17] S. Delfino, A. Saccone, R. Ferro, Metall. Trans. A 21 (1990) 2109–2114.
[18] H. Okamoto, J. Phase Equilibria 12 (1991) 249–250.
[19] J.R. Ogren, N.J. Magnani, J.F. Smith, Trans. AIME 239 (1967) 766–771.
[20] J.E. Pahlman, J.F. Smith, Metall. Trans. 3 (1972) 2423–2432.
[21] S. Gorsse, C.R. Hutchinson, B. Chevalier, J.F. Nie, J. Alloys Compd. 392 (2005) 253–262.
[22] C. Guo, Z. Du, Z. Metallkd. 97 (2006) 130–135.
[23] C.P. Guo, Thermodynamic study on Mg-based alloys systems, PhD thesis, University of Science and Technology Beijing, 2007.
[24] F.G. Meng, H.S. Liu, L.B. Liu, Z.P. Jin, Trans. Nonferrous Met. Soc. China 17 (2007) 77–81.
[25] J.T. Mason, P. Chiotti, Metall. Trans. 3 (1972) 2851–2855.
[26] H.Y. Qi, Z.P. Jin, L.B. Liu, H.S. Liu, J. Alloys Compd. 458 (2008) 184–188.
[27] H.O. Li, X.P. Su, Y. Liu, Z. Li, X.M. Wang, J. Alloys Compd. 457 (2008) 344–347.
[28] X.J. Liu, X. Chen, C.P. Wang, J. Alloys Compd. 468 (2009) 115–121.
[29] M.E. Drits, E.M. Padezhnova, N.V. Miklina, Izvest. VUZ Tsvetnaya Met. 4 (1971) 103–107.
[30] M.E. Drits, E.M. Padezhnova, N.V. Miklina, Technol. Legk. Splavov 2 (1971) 32–35.
[31] M.E. Drits, E.M. Padezhnova, N.V. Miklina, Izv. Akad. Nauk SSSR, Met. 3 (1974) 225–229.
[32] V.V. Kinzhibalo, A.T. Tyvanchuk, E.V. Melnik, Stable and Metastable Phase Equilibria in Metallic Systems, Nauka, Moscow, USSR, 1985, pp. 70–74.
[33] M.L. Huang, J.Y. Yang, H.X. Li, Y.P. Ren, H. Ding, S.M. Hao, J. Mater. Metall. 7 (2008) 126–142.
[34] M.L. Huang, H.X. Li, J.Y. Yang, Y.P. Ren, H. Ding, S.M. Hao, Acta Metall. Sin. 44 (2008) 385–390.
[35] M.L. Huang, H.X. Li, H. Ding, Z.Y. Tang, R.B. Mei, H.T. Zhou, R.P. Ren, S.M. Hao, J. Alloys Compd. 489 (2010) 620–625.
[36] SGTE Pure Elements (Unary) Database (version v 4.6), developed by SGTE (Scientific Group Thermodata Europe), 1991–2008, and provided by TCSAB (January 2008). SGTE website, http://www.sgte.org.
[37] O. Redlich, A.T. Kister, Ind. Eng. Chem. 40 (1948) 345–348.
[38] B. Sundman, J. Ågren, J. Phys. Chem. Solids 42 (1981) 297–307.
[39] I. Ansara, N. Dupin, H.L. Lukas, B. Sundman, J. Alloys Compd. 247 (1997) 20–30.